Packet Error Probability and Effective Throughput for Ultra-Reliable and Low-Latency UAV Communications

Kezhi Wang, *Senior Member, IEEE*, Cunhua Pan, *Member, IEEE*, Hong Ren, Wei Xu, *Senior Member, IEEE*, Lei Zhang, *Senior Member, IEEE*, and Arumugam Nallanathan, *Fellow, IEEE*

***Abstract*— In this paper, we study the average packet error probability (APEP) and effective throughput (ET) of the control link in unmanned-aerial-vehicle (UAV) communications, where the ground central station (GCS) sends control signals to the UAV that requires ultra-reliable and low-latency communications (URLLC). To ensure the low latency, short packets are adopted for the control signal. As a result, the Shannon capacity theorem cannot be adopted here due to its assumption of infinite channel blocklength. We consider both free space (FS) and 3-Dimensional (3D) channel models by assuming that the locations of the UAV are randomly distributed within a restricted space. We first characterize the statistical characteristics of the signal-to-noise ratio (SNR) for both FS and 3D models. Then, the closed-form analytical expressions of APEP and ET are derived by using Gaussian-Chebyshev quadrature. Also, the lower bounds are derived to obtain more insights. Finally, we obtain the optimal value of packet length with the objective of maximizing the ET by applying one-dimensional search. Our analytical results are verified by the Monte-Carlo simulations.**

***Index Terms*— UAV, URLLC, packet error probability, effective throughput, short packet transmission.**

I. Introduction

UNMANNED aerial vehicle (UAV) communication has attracted increasingly attention from both industry and academia [1]. Compared with the conventional terrestrial communications, UAV can be deployed in a swift and flexible way on demands. For example, it can be used to offload heavy data load in hot spot area, and provide temporary communication services when public communication infrastructure is damaged due to nature disasters. In addition, UAV can act as a relay when there is no reliable direct communication links between distant nodes. The channel quality between the UAV and ground users can be enhanced due to the higher probability of short-distance line-of-sight (LoS) links. For instance, the enhancement of cell-edge communications via the UAVs served as the mobile relay was studied in multi-cell networks [2], where the ground centres first send information to the UAVs and then the UAVs forward the received data to the user based on the association scheme.

UAV trajectory design has been studied in [3]–[5]. In particular, Zeng *et al.* studied the throughput maximization problem by jointly optimizing transmission power and UAV trajectory for mobile relay system. The energy consumption of fixed-wing UAVs was derived in [4], based on which energy efficiency was maximized subject to the constraints of UAV speed and acceleration. Then, Wu *et al.* extended [3], [4] to a multi-UAV enabled communication system, and the fairness issue was studied by jointly optimizing user association, UAV trajectory and power control. The other research line is UAV location/placement optimization for static-UAV enabled wireless networks [6]–[8]. Specifically, Hourani *et al.* [6] provided an analytical approach to optimize the altitude of UAV to provide maximum radio coverage on ground users. The circle packing theory was adopted in [7] to optimize the locations of multiple UAVs. Alzenad *et al.* [8] proposed an optimal placement algorithm for maximizing the number of covered users using the minimum transmit power. Furthermore, UAV served as mobile edge computing (MEC) have been studied in [9], [10]. In [9], a secure UAV system has been studied where multiple ground users offload the tasks to the UAV-enabled MEC system in the presence of several eavesdropping UAVs. In [10], large-scale mobile users was considered in the multi-UAV enabled MEC, where offloading decision and resource allocation were studied.

However, all the above works mainly focused on the conventional data transmission without considering the control communication links which require much more stringent latency and higher reliability in order to avoid collision and crash. The control communication link generally requires low data rate for exchanging safety-critical signals. To ensure the extremely

Manuscript received January 19, 2020; revised July 11, 2020; accepted September 11, 2020. Date of publication September 21, 2020; date of current version January 15, 2021. The work of W. Xu was supported in part by the Natural Science Foundation of Jiangsu Province for Distinguished Young Scholars under Grant BK20190012, and the NSFC under grants 61871109 and 61941115; The work of L. Zhang was supported in part by the U.K. Engineering and Physical Sciences Research Council (EP/S02476X/1). The associate editor coordinating the review of this article and approving it for publication was J. Choi. *(Corresponding author: Cunhua Pan.)*

Kezhi Wang is with the Department of Computer and Information Sciences, Northumbria University, Newcastle upon Tyne NE1 8ST, U.K. (e-mail: kezhi.wang@northumbria.ac.uk).

Cunhua Pan, Hong Ren, and Arumugam Nallanathan are with the School of Electronic Engineering and Computer Science, Queen Mary University of London, London E1 4NS, U.K. (e-mail: c.pan@qmul.ac.uk; h.ren@qmul.ac.uk; a.nallanathan@qmul.ac.uk).

Wei Xu is with the National Mobile Communications Research Laboratory, Southeast University, Nanjing 210096, China, and also with Purple Mountain Laboratories, Nanjing 211111, China (e-mail: wxu@seu.edu.cn).

Lei Zhang is with the School of Engineering, University of Glasgow, Glasgow G12 8QQ, U.K. (e-mail: lei.zhang@glasgow.ac.uk).

Color versions of one or more of the figures in this article are available online at https://ieeexplore.ieee.org.

Digital Object Identifier 10.1109/TCOMM.2020.3025578

low latency (e.g., 1 ms), short packet (e.g., 20 bytes) should be adopted [11]. Thus the Shannon capacity formula based on the philosophy of the law of large numbers does not guarantee an asymptotically reliable communication. Therefore non-negligible packet error probability exists and effective throughput may drop. In [12], the authors derived the maximum range between UAVs and a ground control station such that the transmission delay and the overall packet loss probability requirement can be guaranteed. In [13], the UAV serves as a relay to provide URLLC services between the controller and the robot. In [14], UAV-enabled relay communication system were studied for delivering URLLC messages, where the UAV is operating under amplifier-and-forward (AF) mode.

However, there is a paucity of contributions devoted to the performance analysis in UAV-URLLC communication systems. In [15], the approximate closed-form expression of the packet error probability in finite blocklength regime has been derived, which is an involved function of packet length/channel uses, signal-to-noise ratio (SNR) and packet size. This calls for a complete paradigm shift to the study of average packet error probability performance (APEP) and effective throughput (ET) in UAV communications.

Against the above background, the contributions of this paper are summarised as follows:

1) We characterize the statistical characteristics of the signal-to-noise ratio (SNR) for both free space (FS) and 3-dimensional (3D) models by assuming that the UAV flies freely in a restricted area. We consider the randomness of the locations of UAV by using the stochastic geometry theory. Both FS and 3D channel models are considered, where FS is used for the environment where the line-of-sight (LoS) dominates, whereas 3D model is applied to the scenario where the None-LoS (NLoS) cannot be ignored such as urban areas.
2) We then study the average packet error probability (APEP) and effective throughput (ET) under short packet transmission of the control link from ground control station (GCS) to UAV. The Gaussian-Chebyshev quadrature method is adopted to derive the closed-form expression of APEP and ET under short packet transmission, which can provide engineering insights on the packet size design and more understanding of the packet error rate incurred in transmission.
3) Then, closed-form lower bounds are derived for APEP and ET under both FS and 3D channel models by using the convexity of error expression and Jensen's inequality. Also, upper bound is derived for APEP and ET under FS model with insights given to the practical system design. Moreover, the optimal value of packet length with the objective of maximizing the ET under FS and 3D is provided by applying one-dimensional search.
4) Finally, Monte-Carlo simulations are conducted to demonstrate the correctness of our derived results, and show the tightness of the analytical expressions under different conditions.

The rest of this paper is organized as follows. In Section II, we first introduce the system model including FS, 3D channel model and the point-to-point short packet transmission theory.

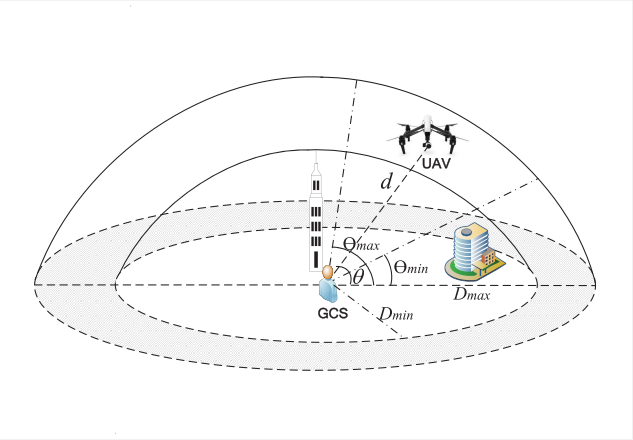

Fig. 1. Illustration of the low-latency transmission of control information from GCS to a UAV.

In Section III, the exact, lower and upper bound are derived for APEP and ET under FS channel model, whereas the exact and lower bound are studied for APEP and ET under 3D channel model in Section IV. Also, the optimal value of packet length with the objective of maximizing the ET under FS and 3D are shown in Section III and IV, respectively. Simulation results and analysis are shown in Section V. Finally, the paper is concluded in Section VI.

II. System Model

We consider a UAV network where a GCS sends control signals to a UAV, which has stringent QoS requirements in terms of ultra-high reliability and ultra-low latency, as shown in Fig. 1. For simplicity, both GCS and UAV are assumed to be equipped with one antenna. The GCS is also assumed to be located at the center of the sphere. Two hemispheres are introduced that share the same center point at the GCS. The UAV is assumed to be within the outer hemisphere to ensure that the UAV is within the control range of the GCS. In addition, we assume that the UAV will not fly into the inner hemisphere. The assumption is reasonable since there may be some obstacles or buildings around the GCS. The radius of the inner and outer hemisphere are denoted as D_{min} and D_{max}, respectively. The UAV is assumed to fly freely within the space specified by the two hemispheres as shown in Fig. 1. As the UAV may fly anywhere within the restricted space, we assume the distance d between UAV and GCS is uniformly distributed in the restricted area. This assumption has also been applied in other work, e.g., [16], [17]. Then, the cumulated distribution function (CDF) of d can be calculated as [17]:

$$F_d(x) = \begin{cases} \dfrac{x^3 - D_{min}^3}{D_{max}^3 - D_{min}^3}, & D_{min} \le x \le D_{max}, \\ 1, & x > D_{min}. \end{cases} \tag{1}$$

and the probability distribution function (PDF) of d is

$$f_d(x) = \begin{cases} \dfrac{dF_d(x)}{dx} = \dfrac{3x^2}{D_{max}^3 - D_{min}^3}, & D_{min} \le x \le D_{max}, \\ 0, & \text{otherwise.} \end{cases} \tag{2}$$

A. Channel Model

Two channel models are considered as follows:

1) Free-Space (FS) Channel Model: This channel is the simplest channel model, which is for the scenario where the LoS dominates the environment, i.e., in less crowded areas. The channel gain from the GCS to the UAV mainly depends on the GCS-UAV distance and the antenna gain. Then, the channel power gain from GCS to UAV follows the FS path loss model, which can be expressed as $h = \beta d^{-2}$ [18], where d is the GCS-UAV distance and β is the channel power at the reference distance of 1 m that is related to the antenna gain. This channel model is valid when the UAV is deployed in an obstacle-free area, such as big square, play ground, large lawn, etc. We assume that the transmission power from the GCS to the UAV is fixed as P and the noise power at the UAV is denoted as σ^2. Then, the SNR at UAV is given by

$$\gamma^{FS} = \lambda d^{-2} \tag{3}$$

where $\lambda = P\beta/\sigma^2$.

2) 3D Channel Model: We adopt the 3D channel model proposed in [6] which is more practical than above free space channel model for urban areas with dense obstacles such as buildings and trees. In this model, both LoS and NLoS links are considered. The probability of having a LoS connection between the GCS and the UAV is given by [6]

$$P_{\mathrm{LoS}} = \frac{1}{1 + a\exp\left(-b\left(\theta - a\right)\right)}, \tag{4}$$

where a and b are positive constants that depend on the environment and the values are given in [6], θ is the elevation angle given by $\theta = \arctan\frac{h}{g}$ [1] with h denoting the altitude of the UAV and g horizontal distance between the UAV and the GCS. The probability of NLoS is $P_{\mathrm{NLoS}} = 1 - P_{\mathrm{LoS}}$. Also, one can get the PDF of θ as

$$f_\theta(x) = \frac{1}{\Theta_{max} - \Theta_{min}} \tag{5}$$

and the CDF of θ as

$$F_\theta(x) = \frac{x - \Theta_{min}}{\Theta_{max} - \Theta_{min}}. \tag{6}$$

The channel path loss models for LoS and NLoS links shown in dB are [6]

$$L_{\mathrm{k}} = 20\log_{10}\left(\frac{4\pi f_c d}{c}\right) + \eta_{\mathrm{k}}, \mathrm{k} \in \{\mathrm{LoS}, \mathrm{NLoS}\} \tag{7}$$

where the first term corresponds to the free space path loss, and η_{LoS} and η_{NLoS} are the additional path loss for LoS and NLoS, respectively. Note that the effect of shadowing has already been included in the path loss model for the non-line-of-sight link η_{NLoS} [6]. In general, η_{NLoS} is much larger than η_{LoS} due to the severe path loss of NLoS. Then, for a given location of UAV, we consider the mean path loss by considering the probability of both LoS and NLoS links:

$$L(\theta, d) = L_{\mathrm{LoS}} P_{\mathrm{LoS}} + L_{\mathrm{NLoS}} P_{\mathrm{NLoS}}. \tag{8}$$

[1] θ here means the degrees of the angle and its value ranges from 0 to 90.

By substituting (4) and (7) into (8), the mean path loss in (8) can be rewritten as

$$L(\theta, d) = \frac{A}{1 + a\exp\left(-b\left(\theta - a\right)\right)} + 20\log_{10}\left(d\right) + C, \tag{9}$$

where A and C are constants given by $A = \eta_{\mathrm{LoS}} - \eta_{\mathrm{NLoS}}$ and $C = 20\log_{10}\left(\frac{4\pi f_c}{c}\right) + \eta_{\mathrm{NLoS}}$, respectively.

Assume that the transmission power from GCS to UAV is fixed as P and the noise power at UAV is denoted as σ^2, then the signal-to-noise ratio (SNR) at the UAV is as [6], [17]

$$\begin{aligned}\gamma^{3D} &= \frac{P}{\sigma^2} 10^{-\frac{L(\theta,d)}{10}} \\ &= \tilde{C} d^{-2} e^{\frac{\tilde{A}}{1 + a\exp(-b(\theta - a))}} \\ &= \hat{d}\hat{\theta}\end{aligned} \tag{10}$$

where $\hat{d} = \tilde{C} d^{-2}$, $\hat{\theta} = e^{\frac{\tilde{A}}{1 + a\exp(-b(\theta - a))}}$, $\tilde{A} = -A\frac{\ln 10}{10} > 0$ and $\tilde{C} = \frac{P}{\sigma^2} e^{-\frac{C\ln 10}{10}}$.

B. Point-to-Point Short Packet Transmission Theory

Let us define the coding rate, R, as the ratio of the number of information bits to the total number of bits per channel use. According to [19], the Shannon capacity is defined as the maximum coding rate for which an arbitrarily low packet error probability is achievable for a sufficiently large number of codewords. However, for the control signal transmission, the packet length, or the number of codewords, should be small to ensure the stringent latency requirement. Thus, the Shannon capacity theorem cannot be adopted here due to its assumption of infinite channel blocklength.

We assume that the packet size of the control signal is L bits, which should be transmitted within $T_{\max}$ seconds. Then, the number of bits per channel use is given by $M = B \cdot T_{\max}$ [20], where B denotes the system bandwidth. Thus, the coding/data rate is given by $R = L/M$. According to [20], a very tight approximation of the packet error probability for a point-to-point transmission under finite blocklength transmission region is given by

$$\varepsilon = Q\left(f\left(\gamma\right)\right), \tag{11}$$

where the notation ε can be either ε^{FS} or ε^{3D} for FS or 3D scenarios, respectively; γ can be either γ^{FS} or γ^{3D} for FS or 3D scenarios, respectively; $f\left(\gamma\right) = \sqrt{\frac{M}{V(\gamma)}}\left(\ln(1+\gamma) - R_s\right)$, $R_s = \frac{L\ln 2}{M}$ (nats per channel use, or npcu), $V(\gamma)$ is the channel dispersion that is given by $V(\gamma) = 1 - (1+\gamma)^{-2}$ [15], and $Q\left(x\right)$ is the Gaussian Q-function given by $Q\left(x\right) = \frac{1}{\sqrt{2\pi}}\int_x^\infty e^{-\frac{t^2}{2}}\mathrm{d}t$. The expression of (11) can be interpreted as follows: ε is minimum packet error probability for which there exists an encoder/decoder pair to transmit L information bits within M bits per channel use.

Also, the ET can be given by

$$\eta = R_s\left(1 - \varepsilon\right) \tag{12}$$

where η can be either η^{FS} or η^{3D} for FS or 3D scenarios, respectively.

In the following, we will derive the APEP and ET by considering the randomness of the UAV location in the restricted area, under both FS and 3D scenarios. The complicated expression of ε in (11), especially the expression of $V(\gamma)$, makes the analysis of APEP and ET a challenging task. Next, the APEP and ET are derived for FS and 3D channel models in Section III and IV, respectively.

III. APEP and ET Under Free-Space Channel Model

A. PDF of γ^{FS}

In this section, we aim to derive the APEP under free-space channel model by transmitting a packet with fixed size of L. Specifically, the APEP in this case is defined as

$$\bar{\varepsilon}^{FS} = \mathbb{E}\{\varepsilon^{FS}\} = \int_{D_{min}}^{D_{max}} \varepsilon^{FS} f_d(x) dx, \tag{13}$$

where $f_d(x)$ is the PDF of d that can be obtained from (1), and γ^{FS} in ε^{FS} is provided in (3) and (11) respectively.

To reduce the analysis complexity, we consider the PDF of γ^{FS} in the following Lemma.

Lemma 1: The PDF of SNR γ^{FS} denoted as $f_{\gamma^{FS}}(x)$ is given by [17]

$$f_{\gamma^{FS}}(x) = \begin{cases} \dfrac{3x^{-\frac{5}{2}}\lambda^{3/2}}{2(D_{max}^3 - D_{min}^3)}, & \gamma_{min}^{FS} \le x \le \gamma_{max}^{FS} \\ 0, & \text{otherwise,} \end{cases} \tag{14}$$

where $\gamma_{min}^{FS} = \frac{\lambda}{D_{max}^2}$ and $\gamma_{max}^{FS} = \frac{\lambda}{D_{min}^2}$.

Proof: Please refer to Appendix A. ∎

Moreover, when $D_{min} = 0$, one has $f_{\gamma^{FS}}(x) = \frac{3x^{-\frac{5}{2}}(\lambda^{FS})^{3/2}}{2D_{max}^3}, x \ge \gamma_{min}^{FS}$. This can be seen as the case where there is no obstacle between the control centre and UAV and also UAV may fly back to the control centre.

B. Chebyshev Approximation

By using (11) and (14), APEP can be re-expressed as

$$\begin{aligned} \bar{\varepsilon}^{FS} &= \int_{\gamma_{min}^{FS}}^{\gamma_{max}^{FS}} Q\left(\sqrt{\frac{M}{V(x)}}\left(\ln(1+x) - R_s\right)\right) f_{\gamma^{FS}}(x) dx \\ &= \frac{3\lambda^{3/2}}{4(D_{max}^3 - D_{min}^3)} \\ &\quad \cdot \int_{\gamma_{min}^{FS}}^{\gamma_{max}^{FS}} \text{erfc}\left(\frac{1}{\sqrt{2}}\sqrt{\frac{M}{V(x)}}\left(\ln(1+x) - R_s\right)\right) x^{-\frac{5}{2}} dx, \end{aligned} \tag{15}$$

where γ_{min}^{FS} and γ_{max}^{FS} are given in Lemma 1, and the last equality follows by using the relationship of $\text{erfc}(x) = 2Q(\sqrt{2}x)$. To the best of our knowledge, it is very difficult to find the closed-form expression of (15), if not impossible.

Next, we apply Gaussian-Chebyshev quadrature to address this issue by using [21, Eq. (25.4.30)]. Let us first define

$$q^{FS}(x) = \text{erfc}\left(\frac{1}{\sqrt{2}}\sqrt{\frac{M}{V(x)}}\left(\ln(1+x) - R_s\right)\right) x^{-\frac{5}{2}}. \tag{16}$$

Then, one can have

$$\begin{aligned} \int_{\gamma_{min}^{FS}}^{\gamma_{max}^{FS}} q^{FS}(x) dx &\approx \frac{\gamma_{max}^{FS} - \gamma_{min}^{FS}}{2} \\ &\quad \cdot \sum_{i=1}^{N} a_i q^{FS}\left(\frac{\gamma_{max}^{FS} - \gamma_{min}^{FS}}{2} t_i + \frac{\gamma_{max}^{FS} + \gamma_{min}^{FS}}{2}\right), \end{aligned} \tag{17}$$

where t_i is the i-th zero of Legendre polynomials, N is the number of terms, a_i is the Gaussian weight given by Table (25.4) of [21]. By substituting (17) into (15), one can have

$$\begin{aligned} \bar{\varepsilon}^{FS} &\approx \frac{3\lambda^{3/2}(\gamma_{max}^{FS} - \gamma_{min}^{FS})}{8(D_{max}^3 - D_{min}^3)} \\ &\quad \times \sum_{i=1}^{N} a_i \cdot q^{FS}\left(\frac{\gamma_{max}^{FS} - \gamma_{min}^{FS}}{2} t_i + \frac{\gamma_{max}^{FS} + \gamma_{min}^{FS}}{2}\right) \\ &\triangleq \bar{\varepsilon}_C^{FS}. \end{aligned} \tag{18}$$

With the increase of N, the accuracy of the above expression will be increased, but at the cost of more computations. To obtain more insights, we derive the approximate expression of $\bar{\varepsilon}$ in the following section.

Then, by using (18), one can get the ET as

$$\bar{\eta}^{FS} = \mathbb{E}(R_s\left(1 - \gamma^{FS}\right)) = R_s\left(1 - \bar{\varepsilon}^{FS}\right). \tag{19}$$

C. Lower Bound

In the following, we aim to derive the lower bound of the APEP in FS channel model in closed form. To this end, we first introduce the following Lemma.

Lemma 2: ε of (12) is a convex function of γ.

Proof: Please refer to Appendix B. ∎

According to Lemma 2, by employing the Jensen's inequality, we can obtain the lower bound of APEP as follows:

$$\bar{\varepsilon}^{FS} = \mathbb{E}\{\varepsilon(\gamma^{FS})\} \ge \varepsilon(\mathbb{E}\{\gamma^{FS}\}) \triangleq \bar{\varepsilon}_{\text{LB}}^{FS}. \tag{20}$$

To obtain $\bar{\varepsilon}_{\text{LB}}^{FS}$, we only need to calculate $\mathbb{E}\{\gamma^{FS}\}$, which is much easier than directly calculating $\bar{\varepsilon}^{FS}$.

By using (14), one can get $\mathbb{E}\{\gamma^{FS}\}$ as

$$\begin{aligned} \mathbb{E}\{\gamma^{FS}\} &= \int_{\gamma_{min}^{FS}}^{\gamma_{max}^{FS}} f_{\gamma^{FS}}(x) x dx \\ &= \int_{\gamma_{min}^{FS}}^{\gamma_{max}^{FS}} \frac{3\lambda^{3/2} x^{-\frac{5}{2}} \cdot x}{2(D_{max}^3 - D_{min}^3)} dx \\ &= \frac{3\lambda^{3/2}}{\sqrt{\gamma_{max}^{FS}}(D_{max}^3 - D_{min}^3)} - \frac{3\lambda^{3/2}}{\sqrt{\gamma_{min}^{FS}}(D_{max}^3 - D_{min}^3)}. \end{aligned} \tag{21}$$

Then, by using (11) and (20), $\bar{\varepsilon}_{\text{LB}}^{FS}$ can be written as

$$\bar{\varepsilon}_{\text{LB}}^{FS} = \varepsilon\left(\frac{3\lambda}{D_{max}^2 + D_{min}^2 + D_{max}D_{min}}\right). \tag{22}$$

Similarly, ET can be expressed as

$$\begin{aligned} \bar{\eta}_{LB}^{FS} &= R_s\left(1 - \bar{\varepsilon}_{LB}^{FS}\right) \\ &= R_s\left(1 - \varepsilon\left(\frac{3\lambda}{D_{max}^2 + D_{min}^2 + D_{max}D_{min}}\right)\right). \end{aligned} \tag{23}$$

Remark 1: When $\lambda \gg 1$ (i.e., $P/\sigma^2 \gg 1$), $\bar{\varepsilon}_{\mathrm{LB}}^{FS}$ in (22) can be further simplified as

$$\bar{\varepsilon}_{\mathrm{LB}}^{FS} = Q\left(\sqrt{M}\left(\ln\left(K^F\lambda\right) - R_s\right)\right), \tag{24}$$

where $K^F = \frac{3}{D_{max}^2 + D_{min}^2 + D_{max}D_{min}}$.

Proof: Please refer to Appendix C. ■

Remark 2: When $\lambda \gg 1$ (i.e., $P\beta/\sigma^2 \gg 1$), one can have $\bar{\eta}_{LB}^{FS} \to R_s$.

Proof: Please refer to Appendix D. ■

D. Upper Bound

In this section, we provide the upper bound of APEP, which is especially tight in high SNR region when $\lambda \gg 1$.

By using (49) and (50), (15) can be approximated as

$$\begin{aligned}\bar{\varepsilon}_{\mathrm{UB}}^{FS} &= \frac{3\lambda^{3/2}}{4(D_{max}^3 - D_{min}^3)} \\ &\quad \cdot \int_{\gamma_{min}^{FS}}^{\gamma_{max}^{FS}} \mathrm{erfc}\left(\frac{\ln 2 \cdot \sqrt{M}}{\sqrt{2}}\left(\log_2(x) - \frac{L}{M}\right)\right) x^{-\frac{5}{2}} dx \\ &= \frac{3\lambda^{3/2}}{4(D_{max}^3 - D_{min}^3)}\left(u(\gamma_{max}^{FS}) - u(\gamma_{min}^{FS})\right), \end{aligned} \tag{25}$$

where the last equality is obtained by variable substitution and using [22], [23], and function $u(x)$ is given by

$$\begin{aligned} u(x) = &-\frac{2\mathrm{erfc}\left(\frac{M\ln x - L\ln 2}{\sqrt{2}\sqrt{M}}\right)}{3x^{3/2}} - \frac{2}{3}e^{\frac{(L\ln 4 - 3)^2 - 4L^2\ln^2(2)}{8M}} \\ &\cdot \mathrm{erf}\left(\frac{-L\ln 4 + 2M\ln x + 3}{2\sqrt{2}\sqrt{M}}\right). \end{aligned} \tag{26}$$

Remark 3: One can further approximate (25) as

$$\begin{aligned}\bar{\varepsilon}_{\mathrm{UB}}^{FS} \approx &\frac{D_{max}^3}{2\left(D_{max}^3 - D_{min}^3\right)}\left(\mathrm{erfc}\left(\frac{M\ln\left(\frac{\lambda}{D_{max}^2}\right) - L\ln(2)}{\sqrt{2M}}\right)\right. \\ &\left. - \mathrm{erfc}\left(\frac{M\ln\left(\frac{\lambda}{D_{min}^2}\right) - L\ln(2)}{\sqrt{2M}}\right)\right). \end{aligned} \tag{27}$$

Then, one can get the insights that APEP increases with the increase of L, with other parameters fixed.

Proof: Please refer to Appendix E. ■

E. Throughput Maximization

In this subsection, we formulate the throughput maximization problem under the latency constraint as

$$\begin{aligned}\mathcal{P}1: \ &\max_{M} \ \bar{\eta}^{FS} \\ &\text{subject to}: M_{min} \le M \le M_{max}. \end{aligned} \tag{28}$$

By using (19), one can apply the one-dimensional search method to get the optimal solution of $\mathcal{P}1$.

IV. APEP and ET Under 3D Channel Model

In this section, we aim to derive the APEP under 3D channel model. Since we consider the 3D channel model, we introduce the minimum and maximum elevation angle $\Theta_{\min}$ and $\Theta_{\max}$, respectively, so that the UAV will not collide into nearby obstacles such as tall buildings and trees.

A. PDF and CDF of γ^{3D}

In that case, the APEP is given by

$$\bar{\varepsilon}^{3D} = \mathbb{E}\{\varepsilon^{3D}\} = \int_{D_{min}}^{D_{max}} \int_{\Theta_{\min}}^{\Theta_{\max}} \varepsilon^{3D} f_{d,\theta}(x,y) dy dx, \tag{29}$$

where $f_{d,\theta}(x,y)$ is the joint PDF of d and θ, and γ in $\varepsilon(\gamma)$ is given in (10). Since the UAV is randomly deployed in the restricted space in Fig. 1, the PDF of θ is given by (5). In addition, since d and θ are independent, the joint PDF of d and θ are given by

$$f_{d,\theta}(x,y) = f_d(x) f_\theta(y) = \frac{1}{\Theta_{\max} - \Theta_{\min}} \frac{3x^2}{D_{\max}^3 - D_{\min}^3}. \tag{30}$$

The method developed for the free-space channel model cannot be adopted here since double integral needs to be calculated in (13).

Similar to Lemma 1, we derive the PDF of $\hat{d}$ in (10) as

$$f_{\hat{d}}(x) = \frac{3x^{-\frac{5}{2}}\tilde{C}^{3/2}}{2(D_{max}^3 - D_{min}^3)}, \hat{d}_{min} \le x \le \hat{d}_{max}, \tag{31}$$

where $\hat{d}_{min} = \frac{\tilde{C}}{D_{max}^2}$ and $\hat{d}_{min} = \frac{\tilde{C}}{D_{min}^2}$.

Lemma 3: The CDF of $\hat{\theta}$ can be given by

$$F_{\hat{\theta}}(x) = \frac{-\frac{\ln\left(\frac{\tilde{A}}{\ln(x)}^{-1}\right)}{b} + a - \Theta_{\min}}{\Theta_{\max} - \Theta_{\min}}, \hat{\theta}_{min} \le \hat{\theta} \le \hat{\theta}_{max} \tag{32}$$

where $\hat{\theta}_{min} = \exp\left(\frac{\tilde{A}}{a\exp(-b(\Theta_{\min} - a)) + 1}\right)$ and $\hat{\theta}_{max} = \exp\left(\frac{\tilde{A}}{a\exp(-b(\Theta_{\max} - a)) + 1}\right)$.

Proof: Please refer to Appendix F. ■

By taking the first-order derivative of (32) with respect to $\hat{\theta}$, the PDF of $\hat{\theta}$ can be derived as

$$\begin{aligned} f_{\hat{\theta}}(x) = &\frac{\tilde{A}}{bx(\Theta_{\max} - \Theta_{\min})\ln^2(x)\left(\frac{\tilde{A}}{\ln(x)} - 1\right)}, \\ &\hat{\theta}_{min} \le \hat{\theta} \le \hat{\theta}_{max}. \end{aligned} \tag{33}$$

Lemma 4: The PDF of γ^{3D} can be given by

$$f_{\gamma^{3D}}(z) = \begin{cases} W_1(z), & \hat{\theta}_{min} \cdot \hat{d}_{min} \le z \le \hat{\theta}_{min} \cdot \hat{d}_{max} \\ W_2(z), & \hat{\theta}_{min} \cdot \hat{d}_{max} \le z \le \hat{\theta}_{max} \cdot \hat{d}_{min} \\ W_3(z), & \hat{\theta}_{max} \cdot \hat{d}_{min} \le z \le \hat{\theta}_{max} \cdot \hat{d}_{max} \end{cases} \tag{34}$$

where $W_1(z)$, $W_2(z)$ and $W_3(z)$ are given by (54), (55) and (56), respectively.

Proof: Please refer to Appendix G. ■

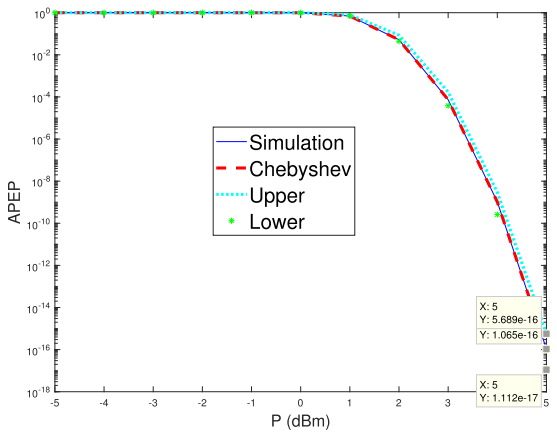

(a) APEP versus P with $M = 100$

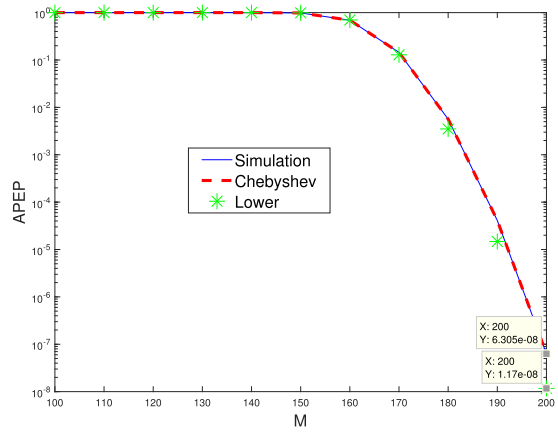

(b) APEP versus M with $P = -5$ dBm

Fig. 2. APEP in FS channel model.

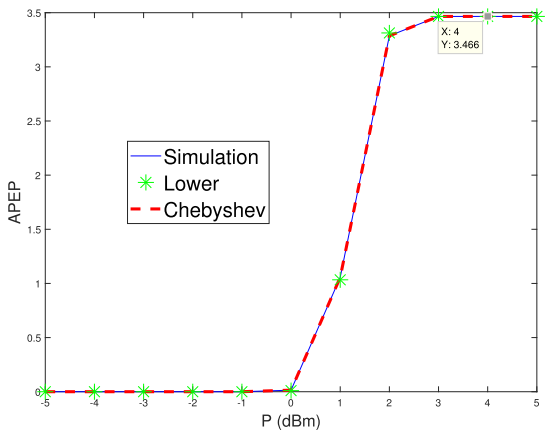

(a) ET versus P with $M = 100$

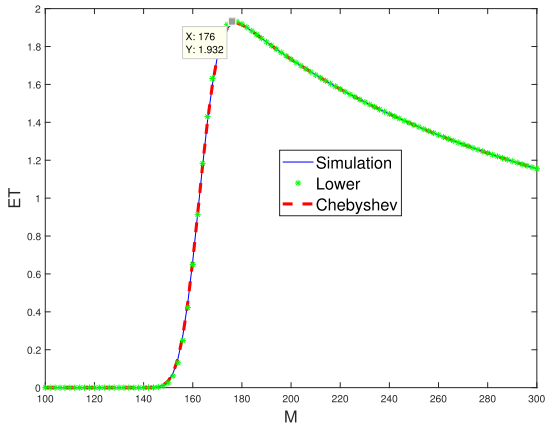

(b) ET versus M with $P = -5$ dBm

Fig. 3. ET in FS channel model.

B. Chebyshev Approximation

In this section, we provide the Chebyshev Approximation to $\bar{\varepsilon}^{3D}$. By using (34), one can get

$$\bar{\varepsilon}^{3D} = \mathbb{E}\{\varepsilon(\gamma^{3D})\} = \int_{\hat{\theta}_{min}\cdot\hat{d}_{min}}^{\hat{\theta}_{min}\cdot\hat{d}_{max}} \varepsilon(z)W_1(z)dz + \int_{\hat{\theta}_{min}\cdot\hat{d}_{max}}^{\hat{\theta}_{max}\cdot\hat{d}_{min}} \varepsilon(z)W_2(z)dz + \int_{\hat{\theta}_{max}\cdot\hat{d}_{min}}^{\hat{\theta}_{max}\cdot\hat{d}_{max}} \varepsilon(z)W_3(z)dz. \quad (35)$$

Let $q_1^{3D}(z) = \varepsilon(z)W_1(z)$, $q_2^{3D}(z) = \varepsilon(z)W_2(z)$ and $q_3^{3D}(z) = \varepsilon(z)W_3(z)$, one can have

$$\bar{\varepsilon}^{3D} \approx \sum_{i=1}^{N} a_i \cdot q_1^{3D}\left(\frac{\hat{\theta}_{min}\cdot\hat{d}_{max} - \hat{\theta}_{min}\cdot\hat{d}_{min}}{2}t_i + \frac{\hat{\theta}_{min}\cdot\hat{d}_{max} + \hat{\theta}_{min}\cdot\hat{d}_{min}}{2}\right) + \sum_{i=1}^{N} a_i \cdot q_2^{3D} \cdot \left(\frac{\hat{\theta}_{max}\cdot\hat{d}_{min} - \hat{\theta}_{min}\cdot\hat{d}_{max}}{2}t_i + \frac{\hat{\theta}_{max}\cdot\hat{d}_{min} + \hat{\theta}_{min}\cdot\hat{d}_{max}}{2}\right) + \sum_{i=1}^{N} a_i \cdot q_3^{3D}\left(\frac{\hat{\theta}_{max}\cdot\hat{d}_{min} - \hat{\theta}_{max}\cdot\hat{d}_{min}}{2}t_i + \frac{\hat{\theta}_{max}\cdot\hat{d}_{min} + \hat{\theta}_{max}\cdot\hat{d}_{min}}{2}\right). \quad (36)$$

One can see that with the increase of N, the accuracy of the above expression will be increased, but at the cost of more computations. Then, by using (12) and (36), one can obtain the ET as

$$\bar{\eta}^{3D} = R_s\left(1 - \bar{\varepsilon}^{3D}\right). \quad (37)$$

C. Lower Bound

Similarly, the lower bound of APEP can be given by

$$\bar{\varepsilon}^{3D} = \mathbb{E}\{\varepsilon(\gamma^{3D})\} \geq \varepsilon(\mathbb{E}\{\gamma^{3D}\}) \triangleq \bar{\varepsilon}_{\mathrm{LB}}^{3D}. \quad (38)$$

Remark 4: $\bar{\varepsilon}_{\mathrm{LB}}^{3D}$ can be given by

$$\bar{\varepsilon}_{\mathrm{LB}}^{3D} = \varepsilon(U_1 + U_2 + U_3), \quad (39)$$

where U_1, U_2 and U_3 are given by (58), (59) and (60), respectively.

Proof: Please refer to Appendix H. ∎

Similarly, ET can be expressed as

$$\bar{\eta}_{LB}^{3D} = R_s\left(1 - \bar{\varepsilon}_{LB}^{3D}\right) = R_s\left(1 - \varepsilon\left(U_1 + U_2 + U_3\right)\right). \quad (40)$$

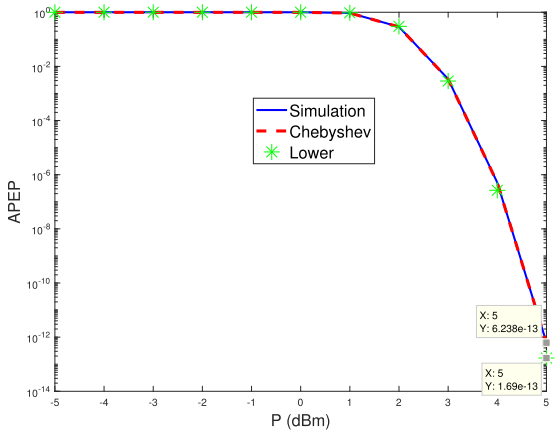

(a) Suburban

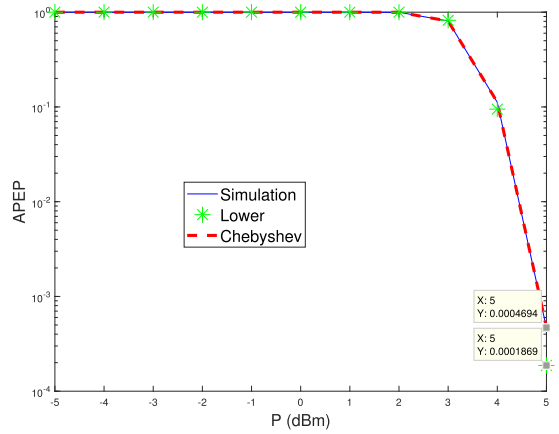

(b) Dense Urban

Fig. 4. APEP versus P with $M = 100$.

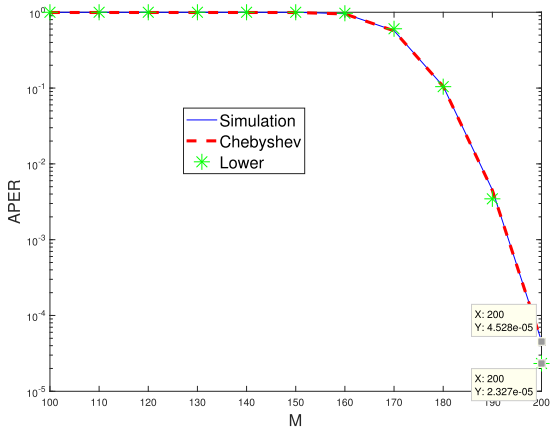

(a) Suburban

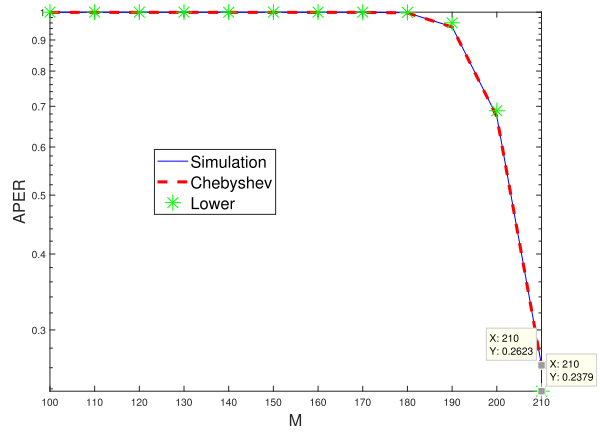

(b) Dense Urban

Fig. 5. APEP versus M with $P = -5$ dBm.

Remark 5: When $\tilde{C} \gg 1$, i.e., $P/\sigma^2 \gg 1$, one can have $\bar{\eta}_{LB}^{3D} \to R_s$.

Proof: Please refer to Appendix I. ■

D. Throughput Maximization

In this subsection, we consider the throughput maximization under the latency constraint as follows

$$\mathcal{P}2: \max_{M} \bar{\eta}^{3D} \quad \text{subject to}: M_{min} \leq M \leq M_{max}. \tag{41}$$

It is very difficult to obtain the closed-form solution of M^*, if not impossible. Thus, similar with before, by using (37), one may apply the one-dimensional search method to get the optimal solution of $\mathcal{P}2$.

V. Numerical Results

In this section, simulation results are presented to verify the correctness of our derived results in this paper. Unless otherwise stated, the simulation parameters are set as follows: $D_{min} = 900$ m, $D_{max} = 950$ m, $B = 1$ MHz, $L = 500$ and $\sigma^2 = -173$ dBm/Hz. In FS scenario, we set $\beta = -40$ dB. In 3D case, we set $f_c = 2.5$ GHz, $c = 3 \cdot 10^8$ m/s and $\Theta_{\max} = 90$. Two scenarios are considered: dense urban and suburban. The values of the corresponding parameters can be found in [24]. $\Theta_{\min}$ is set to be 70 and 30 for dense urban and suburban, respectively. The other parameters are specified in each simulation figure. The curve labelled 'Simulation' is obtained by randomly and uniformly deploying the UAV in the specified region for 10000 times. The curve labelled 'Chebyshev' is obtained by using (18) in FS and (36) in 3D scenario. The curve labelled 'Upper' is obtained by using (27) in FS. Also, the curve labelled 'Lower' is obtained by using (22) in FS and (39) in 3D scenario.

A. FS Channel Model

In Fig. 2, we plot the APEP versus P in Fig. 2 (a) with the packet length given by $M = 100$, and APEP versus M in Fig. 2 (b) with the power given by $P = -5$ dBm. It is observed from Fig. 2 (a) that the APEP with finite blocklength regime decreases with the increase of P as expected. Also, one can see from Fig. 2 (b) that the APEP decreases with the increase of M as well, which confirms the conclusion from Remark 1. From Fig. 2, one can see that our derived Chebyshev curve approximates the exact result very well. The performance gap between the simulation and the derived lower bound as well as upper bounds are small, which is $0.954e$-16 and $4.624e$-16, respectively in the case of P = 5dBm. Hence, these results can

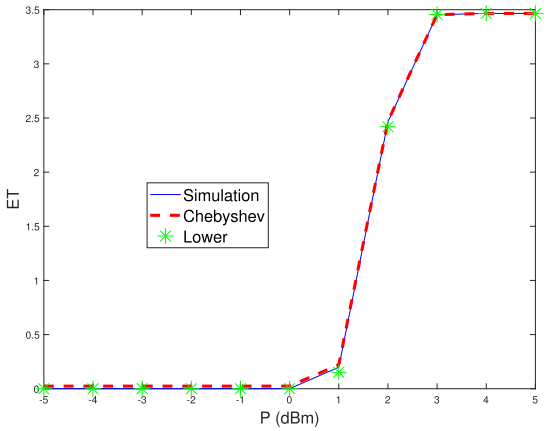

(a) Suburban

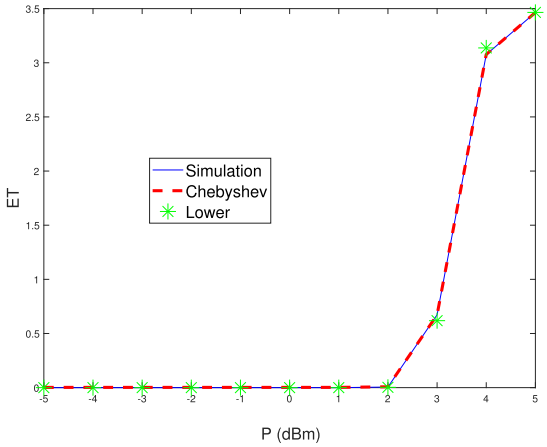

(b) Dense Urban

Fig. 6. ET versus P with $M = 100$.

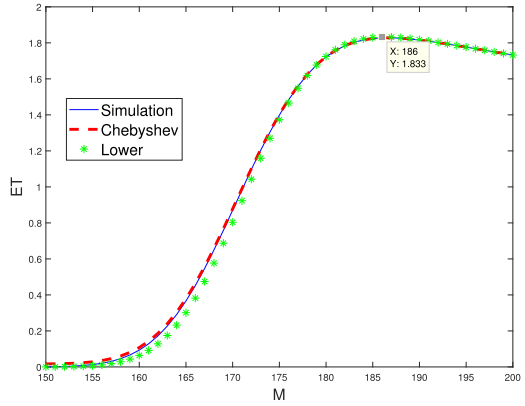

(a) Suburban

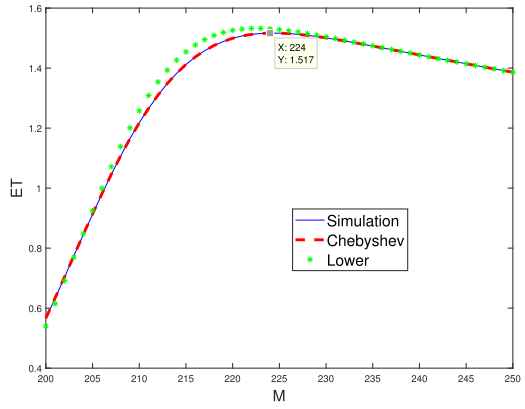

(b) Dense Urban

Fig. 7. ET versus M with $P = -5$ dBm.

be used to analyse the trend of the APEP. When the SNR value P is set to 5 dBm, the APEP can be as low as 10^{-16}. Also, it is noted that when the packet length M reaches 200, APEP can be as low as 10^{-7}, which satisfies the extremely reliability requirement for control signal transmission.

In Fig. 3, we plot the ET versus P in Fig. 3 (a) with the packet length given by $M = 100$, and ET versus M in Fig. 3 (b) with the power given by $P = -5$ dBm. One can see from Fig. 3 (a) that the ET increase with the increase of P, as expected. Also, one can see that the value of ET reaches the roof, i.e., $R_s = 3.466$ with the further increase of P, which can also be derived from Remark 2.

In Fig. 3 (b), one sees that ET first increases and then decreases with the increase of M. The optimal value can be reached when M is 176, by applying one-dimensional search.

B. 3D

In Fig. 4, we plot the APEP versus P in 3D scenario with the packet length $M = 100$, where Fig. 4 (a) describes suburban area while Fig. 4 (b) shows dense urban area. One can see that the APEP increases with the increase of P for both suburban and dense urban cases, as expected. Also, one can see in dense urban areas, we have worse APEP performance compared with suburban case. Again, one can see that the Chebyshev curve approximates the exact result very well. The performance gap between the simulation and the derived lower bound is small, which can be seen as $0.954e$-16 and $2.825e$-4 in the case of P = 5dBm in Suburban and Dense Urban areas, respectively.

In Fig. 5, we plot the APEP versus M in 3D scenario with the power of $P = -5$ dBm, where Fig. 5 (a) shows suburban area while Fig. 5 (b) shows dense urban area. One sees that APEP increases with the increase of M for both suburban and dense urban cases, as expected. Also, one sees in dense urban areas, we have worse APEP compared with suburban case.

In Fig. 6, we plot the ET versus P in 3D scenario with the packet length $M = 100$, where Fig. 6 (a) shows suburban area while Fig. 6 (b) shows dense urban area. One can see that the ET increase with the increase of P for both suburban and dense urban cases, as expected. Also, one can see in dense urban areas, we have worse ET compared with suburban area in the same parameter settings.

Additionally, one can see that with the increase of P, ET reaches its upper floor 3.47 for both cases, which verifies Remark 5.

In Fig. 7, we plot the ET versus M in 3D scenario with the power of $P = -5$ dBm, where Fig. 7 (a) shows suburban area while Fig. 7 (b) shows dense urban area. One can see that ET first increases and then decreases with the increase of M for both cases. One can obtain that the optimal values of M are 186 for suburban and 224 for dense urban scenarios, by applying the one-dimensional search.

VI. Conclusion

In this paper, we have studied the APEP and ET for the GCS-to-UAV control link communication under the short packet transmission regime to enable the stringent latency and reliable requirements. For the general scenarios in FS and 3D, we have derived an accurate approximate expression of the APEP and ET by using the Gaussian-Chebyshev quadrature method. To obtain more insights, lower bound of APEP and ET for both FS and 3D scenarios have been derived. Moreover, the optimal value of packet length with the objective of maximizing the ET has been obtained by applying the one-dimensional search.

The future work will focus on multi-UAVs scenario and more general results are expected to obtain in both FS and 3D channel models.

Appendix A
Proof of Lemma 1

The CDF of γ can be given by [17]

$$F_{\gamma^{FS}}(x) = \Pr\{\gamma^{FS} \le x\} = 1 - \Pr\left\{d \le \left(\frac{\lambda}{x}\right)^{1/2}\right\}. \quad (42)$$

By applying (1) and (42), the CDF of γ^{FS} can be obtained as follows

$$F_{\gamma^{FS}}(x) = \begin{cases} 1 - \dfrac{(\frac{\lambda}{x})^{3/2} - D_{min}^3}{D_{max}^3 - D_{min}^3}, & \gamma_{min}^{FS} \le x \le \gamma_{max}^{FS} \\ 0, & \text{otherwise.} \end{cases} \quad (43)$$

By taking the first-order derivative of (43), the PDF of γ^{FS} can be derived as (14).

Appendix B
Proof of Lemma 2

ε defined in (11) can be regarded as a composition function of Q-function and f-function. For the Q-function $Q(x) = \frac{1}{\sqrt{2\pi}}\int_x^\infty e^{-\frac{t^2}{2}}\mathrm{d}t$, the first-order derivative of $Q(x)$ w.r.t. x can be calculated as $Q'(x) = -\frac{1}{\sqrt{2\pi}}e^{-\frac{x^2}{2}} < 0$, and the second-order derivative is $Q''(x) = \frac{x}{\sqrt{2\pi}}e^{-\frac{x^2}{2}} > 0$ when $x > 0$. For URLLC applications, the decoding error probability is generally much smaller than 0.5, which is equal to $Q(0)$. Since $Q(x)$ is a decreasing function, $x > 0$ always holds. Hence, $Q(x)$ is a decreasing and convex function w.r.t. x. According to the composition rules in [25], $\varepsilon(\gamma)$ is a convex function of γ if $f(\gamma)$ is a concave function of γ, which will be proved in the following.

The first-order derivative of $f(\gamma)$ w.r.t. γ is given by

$$f'(\gamma) = \sqrt{M}\frac{(1+\gamma)^2 - 1 - \left(\ln(1+\gamma) - \frac{L}{M}\ln 2\right)}{\left((1+\gamma)^2 - 1\right)^{\frac{3}{2}}} \quad (44)$$

The second-order derivative of $f(\gamma)$ w.r.t. γ can be calculated as

$$f''(\gamma) = \frac{\sqrt{M}}{\left((1+\gamma)^2 - 1\right)^{\frac{5}{2}}} g(\gamma). \quad (45)$$

where function $g(\gamma)$ is given by

$$g(\gamma) = \left(-(1+\gamma) - \frac{1}{1+\gamma}\right)\left((1+\gamma)^2 - 1\right) + 3(1+\gamma)\left(\ln(1+\gamma) - \frac{L}{M}\ln 2\right). \quad (46)$$

Hence, we need to check the sign of function $g(\gamma)$. The first-order derivative of $g(\gamma)$ w.r.t. γ is given by

$$g'(\gamma) = -3(1+\gamma)^2 - \frac{1}{(1+\gamma)^2} + 3\left(\ln(1+\gamma) - \frac{L}{M}\ln 2\right) + 3. \quad (47)$$

The second-order derivative of $g(\gamma)$ w.r.t. γ is

$$g''(\gamma) = \frac{h(\gamma)}{(1+\gamma)^3}, \quad (48)$$

where $h(\gamma) = -6(1+\gamma)^4 + 2 + 3(1+\gamma)^2$. The first-order derivative of $h(\gamma)$ w.r.t. γ is given by $h'(\gamma) = 6(1+\gamma)\left(1 - 4(1+\gamma)^2\right)$, which is smaller than zero. Hence, $h(\gamma)$ is a monotonically decreasing function. We then have $h(\gamma) < h(0) = -1$. Then, according to (48), we have $g''(\gamma) < 0$, which means $g'(\gamma)$ is also a monotonically decreasing function. Hence, we have $g'(\gamma) < g'(0) = -\frac{L}{M}3\ln 2 - 1 < 0$. Again, this means $g(\gamma)$ is also a monotonically decreasing function. Then, we have $g(\gamma) < g(0) = -\frac{L}{M}3\ln 2 < 0$. By substituting the relation $g(\gamma) < 0$ into (45), we can prove that $f''(\gamma) < 0$, which means $f(\gamma)$ is a concave function, which completes the proof.

Appendix C
Proof of Remark 1

When $x \gg 1$, one has the following approximation

$$\log(1+x) \approx \log(x), \quad (49)$$

and

$$\sqrt{V(x)} = \sqrt{1 - \frac{1}{(x+1)^2}} \approx 1. \quad (50)$$

By using above two approximations, (22) can be written as (24).

Appendix D
Proof of Remark 2

When $\lambda \gg 1$, similar with before, $\bar{\eta}_{LB}^{FS}$ in (23) can be written as

$$\bar{\eta}_{LB}^{FS} = R_s\left(1 - \frac{1}{2}\mathrm{erfc}\left(\sqrt{M/2}\left(\ln\left(K^F\lambda\right) - R_s\right)\right)\right). \quad (51)$$

By using $\mathrm{erf}(x) \to 1$ when $x \to \infty$ and $\mathrm{erfc}(x) = 1 - \mathrm{erf}(x)$, one can get $\bar{\eta}_{LB}^{FS} \to R_s$, which completes the proof.

Appendix E
Proof of Remark 3

In the case of $x \to \infty$ in (26), one has $\mathrm{erf}(x) \to 1$. Therefore, $u(x)$ can be approximated as

$$u(x) \approx -\frac{2\mathrm{erfc}\left(\frac{M\ln(x) - L\ln(2)}{\sqrt{2}\sqrt{M}}\right)}{3x^{3/2}} - \frac{2}{3}e^{\frac{(L\ln(4)-3)^2 - 4L^2\ln^2(2)}{8M}}.$$

Then, after some simple manipulations, one can get (27).

APPENDIX F
PROOF OF LEMMA 3

The CDF of $\hat{\theta}$ can be given by

$$F_{\hat{\theta}}(x) = \Pr\{e^{\frac{\tilde{A}}{1+a\exp(-b(\theta-a))}} \leq x\}. \quad (52)$$

Similar to Appendix A and by applying $F_\theta(x)$ in (6), the CDF of $\hat{\theta}$ can be obtained as (32).

APPENDIX G
PROOF OF LEMMA 4

Without loss of generality, we assume that $\hat{\theta}_{min} \cdot \hat{d}_{max} \leq z \leq \hat{\theta}_{max} \cdot \hat{d}_{min}$ in the following derivations. For other situations, similar derivations can be applied which are omitted here due to space limitation.

By using $f_{\hat{d}}(x)$ in (31) and $f_{\hat{\theta}}(x)$ in (33) and [26], one can get the PDF of γ^{3D} as

$$f_{\gamma^{3D}}(z) = \begin{cases} W_1(z) = \int_{\hat{\theta}_{min}}^{z/\hat{d}_{min}} f_{\hat{\theta}}(x) f_{\hat{d}}(\frac{z}{x})\frac{1}{x}dx, \\ \hat{\theta}_{min}\cdot\hat{d}_{min} \leq z \leq \hat{\theta}_{min}\cdot\hat{d}_{max}; \\ W_2(z) = \int_{z/\hat{d}_{max}}^{z/\hat{d}_{min}} f_{\hat{\theta}}(x) f_{\hat{d}}(\frac{z}{x})\frac{1}{x}dx, \\ \hat{\theta}_{min}\cdot\hat{d}_{max} \leq z \leq \hat{\theta}_{max}\cdot\hat{d}_{min}; \\ W_3(z) = \int_{z/\hat{d}_{max}}^{\hat{\theta}_{max}} f_{\hat{\theta}}(x) f_{\hat{d}}(\frac{z}{x})\frac{1}{x}dx, \\ \hat{\theta}_{max}\cdot\hat{d}_{min} \leq z \leq \hat{\theta}_{max}\cdot\hat{d}_{max}. \end{cases} \quad (53)$$

For $W_1(z)$, by using the variable substitution and [23], [27], one can have

$$\begin{aligned} W_1(z) &= \int_{\hat{\theta}_{min}}^{z/\hat{d}_{min}} f_{\hat{\theta}}(x) f_{\hat{d}}(\frac{z}{x})\frac{1}{x}dx \\ &= \frac{3\tilde{A}\tilde{C}^{3/2}z^{-5/2}}{2b\left(D_{max}^3 - D_{min}^3\right)(\Theta_{\max}-\Theta_{\min})} \\ &\quad \times \int_{\hat{\theta}_{min}}^{z/\hat{d}_{min}} \frac{\sqrt{x}dx}{\tilde{A}\ln(x) - \ln^2(x)} \\ &= \frac{3\tilde{C}^{3/2}z^{-5/2}}{2b\left(D_{max}^3 - D_{min}^3\right)(\Theta_{\max}-\Theta_{\min})} \\ &\quad \times \left(g(\frac{z}{\hat{d}_{min}}) - g(\hat{\theta}_{min})\right) \end{aligned} \quad (54)$$

where $g(x) = \text{Ei}\left(\frac{3\ln(x)}{2}\right) - e^{\frac{3\tilde{A}}{2}}\text{Ei}\left(\frac{3}{2}(\ln(x)-\tilde{A})\right)$ and Ei gives the exponential integral function, defined by $\text{Ei}(z) = -\int_{-z}^{\infty}\frac{e^{-t}}{t}dt$ [23].

Similarly, one can get $W_2(z)$ as

$$W_2(z) = \frac{3\tilde{C}^{3/2}z^{-5/2}}{2b\left(D_{max}^3 - D_{min}^3\right)(\Theta_{\max}-\Theta_{\min})} \cdot\left(g(z/\hat{d}_{min}) - g(z/\hat{d}_{max})\right). \quad (55)$$

Also, one can get $W_3(z)$ as

$$W_3(z) = \frac{3\tilde{C}^{3/2}z^{-5/2}}{2b\left(D_{max}^3 - D_{min}^3\right)(\Theta_{\max}-\Theta_{\min})} \cdot\left(g(\hat{\theta}_{\max}) - g(z/\hat{d}_{max})\right). \quad (56)$$

Then, one can obtain the PDF of γ^{3D} as (34).

APPENDIX H
PROOF OF REMARK 4

$\mathbb{E}\{\gamma^{3D}\}$ can be written as

$$\mathbb{E}\{\gamma^{3D}\} = \underbrace{\int_{\hat{\theta}_{min}\cdot\hat{d}_{min}}^{\hat{\theta}_{min}\cdot\hat{d}_{max}} zW_1(z)dz}_{U_1} + \underbrace{\int_{\hat{\theta}_{min}\cdot\hat{d}_{max}}^{\hat{\theta}_{max}\cdot\hat{d}_{min}} zW_2(z)dz}_{U_2} + \underbrace{\int_{\hat{\theta}_{max}\cdot\hat{d}_{min}}^{\hat{\theta}_{max}\cdot\hat{d}_{max}} zW_3(z)dz}_{U_3}. \quad (57)$$

By using $W_1(z)$ in (54), one can have U_1 as (58), as shown at the top of the next page [23], [28].

Then, by using [23], [28], for U_{11} above, one can have $U_{11} = L_{11}(\hat{\theta}_{min}\cdot\hat{d}_{max}) - L_{11}(\hat{\theta}_{min}\cdot\hat{d}_{min})L_{11}(z) = -\frac{2}{\sqrt{z}}(\text{Ei}(\frac{3}{2}\ln(\frac{D_{max}^2 z}{\tilde{C}})) - \sqrt{\frac{D_{max}^2 z}{\tilde{C}}}\text{li}(\frac{D_{max}^2 z}{\tilde{C}}))$ and $\text{li}(z) = \int_0^z \frac{dt}{\log t}$ denotes the logarithmic integral function [23]; , *where* for U_{12}, one can have $U_{12} = L_{12}(\hat{\theta}_{min}\cdot\hat{d}_{max}) - L_{12}(\hat{\theta}_{min}\cdot\hat{d}_{min})$, where $L_{12}(z) = \frac{2}{\sqrt{z}}e^{\frac{3\tilde{A}}{2}}(e^{-\frac{\tilde{A}}{2}}\sqrt{\frac{D_{max}^2 z}{\tilde{C}}}\text{Ei}(\ln(\frac{D_{max}^2 z}{\tilde{C}}) - \tilde{A}) - \text{Ei}(\frac{-3}{2}(\tilde{A} - \ln(\frac{D_{max}^2 z}{\tilde{C}}))))$; for U_{13}, one can have $U_{13} = L_{13}(\hat{\theta}_{min}\cdot\hat{d}_{max}) - L_{13}(\hat{\theta}_{min}\cdot\hat{d}_{min})$, where $L_{13}(z) = -\frac{2}{\sqrt{z}}\text{Ei}(\frac{3}{2}\ln(e^{\frac{\tilde{A}}{e^{b(a-\Theta_{\min})}a+1}}))$ and for U_{14}, one can have $U_{14} = L_{14}(\hat{\theta}_{min}\cdot\hat{d}_{max}) - L_{14}(\hat{\theta}_{min}\cdot\hat{d}_{min})$, where $L_{14}(z) = -\frac{2}{\sqrt{z}}e^{\frac{3\tilde{A}}{2}}\text{Ei}(\frac{-3}{2}(\tilde{A} - \ln(e^{\frac{\tilde{A}}{e^{b(a-\Theta_{\min})}a+1}})))$.

Similarly, for U_2, one can have

$$U_2 = \frac{3\tilde{C}^{3/2}}{2b\left(D_{max}^3 - D_{min}^3\right)(\Theta_{\max}-\Theta_{\min})} \cdot(U_{21}+U_{22}+U_{23}+U_{24}) \quad (59)$$

where $U_{21} = L_{21}(\hat{\theta}_{max}\cdot\hat{d}_{min}) - L_{21}(\hat{\theta}_{min}\cdot\hat{d}_{max})$, $U_{22} = L_{22}(\hat{\theta}_{max}\cdot\hat{d}_{min}) - L_{22}(\hat{\theta}_{min}\cdot\hat{d}_{max})$, $U_{23} = L_{23}(\hat{\theta}_{max}\cdot\hat{d}_{min}) - L_{23}(\hat{\theta}_{min}\cdot\hat{d}_{max})$, $U_{24} = L_{24}(\hat{\theta}_{max}\cdot\hat{d}_{min}) - L_{24}(\hat{\theta}_{min}\cdot\hat{d}_{max})$, $L_{21}(z) = -\frac{2}{\sqrt{z}}(\text{Ei}(\frac{3}{2}\ln(\frac{D_{max}^2 z}{\tilde{C}})) - \sqrt{\frac{D_{max}^2 z}{\tilde{C}}}\text{li}(\frac{D_{max}^2 z}{\tilde{C}}))$, $L_{22}(z) = \frac{2}{\sqrt{z}}e^{\frac{3\tilde{A}}{2}}[e^{-\frac{\tilde{A}}{2}}\sqrt{\frac{D_{max}^2 z}{\tilde{C}}}\text{Ei}(\ln(\frac{{D_{max}}^2 z}{\tilde{C}}) - \tilde{A}) - \text{Ei}(\frac{-3}{2}(\tilde{A} - \ln(\frac{{D_{max}}^2 z}{\tilde{C}})))]$, $L_{23}(z) = -\frac{2}{\sqrt{z}}(\text{Ei}(\frac{3}{2}\ln(\frac{D_{min}^2 z}{\tilde{C}})) - \sqrt{\frac{D_{min}^2 z}{\tilde{C}}}\text{li}(\frac{D_{min}^2 z}{\tilde{C}}))$ and $L_{24}(z) = \frac{2}{\sqrt{z}}e^{\frac{3\tilde{A}}{2}}[e^{-\frac{\tilde{A}}{2}}\sqrt{\frac{D_{min}^2 z}{\tilde{C}}}\text{Ei}(\ln(\frac{{D_{min}}^2 z}{\tilde{C}}) - \tilde{A}) - \text{Ei}(\frac{-3}{2}(\tilde{A} - \ln(\frac{D_{min}^2 z}{\tilde{C}})))]$.

Similarly, for U_3, one can have

$$U_3 = \frac{3\tilde{C}^{3/2}}{2b\left(D_{max}^3 - D_{min}^3\right)(\Theta_{\max}-\Theta_{\min})}\cdot (U_{31}+U_{32}+U_{33}+U_{34}) \quad (60)$$

where $U_{31} = L_{31}(\hat{\theta}_{max}\cdot\hat{d}_{max}) - L_{31}(\hat{\theta}_{max}\cdot\hat{d}_{min})$, $U_{32} = L_{32}(\hat{\theta}_{max}\cdot\hat{d}_{max}) - L_{32}(\hat{\theta}_{max}\cdot\hat{d}_{min})$, $U_{33} = L_{33}(\hat{\theta}_{max}\cdot\hat{d}_{max}) - L_{33}(\hat{\theta}_{max}\cdot\hat{d}_{min})$, $U_{34} = L_{34}(\hat{\theta}_{max}\cdot\hat{d}_{max}) - L_{34}(\hat{\theta}_{max}\cdot\hat{d}_{min})$, $L_{31}(z) = -\frac{2}{\sqrt{z}}\text{Ei}(\frac{3}{2}\ln(e^{\frac{\tilde{A}}{e^{b(a-\Theta_{\max})}a+1}}))$, $L_{32}(z) = -\frac{2}{\sqrt{z}}e^{\frac{3\tilde{A}}{2}}\text{Ei}(\frac{-3}{2}(\tilde{A} - \ln(e^{\frac{\tilde{A}}{e^{b(a-\Theta_{\max})}a+1}})))$, $L_{33}(z) = -\frac{2}{\sqrt{z}}(\text{Ei}(\frac{3}{2}\ln(\frac{D_{min}^2 z}{\tilde{C}})) - \sqrt{\frac{D_{min}^2 z}{\tilde{C}}}\text{li}(\frac{D_{min}^2 z}{\tilde{C}}))$

$$U_1 = \frac{3\tilde{C}^{3/2}}{2b\left(D_{max}^3 - D_{min}^3\right)\left(\Theta_{\max} - \Theta_{\min}\right)} \cdot \left(\underbrace{\int_{\hat{\theta}_{min}\cdot\hat{d}_{min}}^{\hat{\theta}_{min}\cdot\hat{d}_{max}} z^{-3/2}\mathrm{Ei}\left(\frac{3}{2}\ln\left(\frac{zD_{max}^2}{\tilde{C}}\right)\right)dz}_{U_{11}} \right.$$
$$- \underbrace{\int_{\hat{\theta}_{min}\cdot\hat{d}_{min}}^{\hat{\theta}_{min}\cdot\hat{d}_{max}} e^{\frac{3\tilde{A}}{2}} z^{-3/2}\mathrm{Ei}\left(\frac{-3}{2}\left(\tilde{A} - \ln\left(\frac{z{D_{max}}^2}{\tilde{C}}\right)\right)\right)dz}_{U_{12}} - \underbrace{\int_{\hat{\theta}_{min}\cdot\hat{d}_{min}}^{\hat{\theta}_{min}\cdot\hat{d}_{max}} z^{\frac{-3}{2}}\mathrm{Ei}\left(\frac{3}{2}\ln\left(e^{\frac{\tilde{A}}{a\exp(-b(\Theta_{\min}-a))+1}}\right)\right)dz}_{U_{13}}$$
$$\left. + \underbrace{\int_{\hat{\theta}_{min}\cdot\hat{d}_{min}}^{\hat{\theta}_{min}\cdot\hat{d}_{max}} e^{\frac{3\tilde{A}}{2}} z^{\frac{-3}{2}}\mathrm{Ei}\left(\frac{-3}{2}\left(\tilde{A} - \ln\left(e^{\frac{\tilde{A}}{a\exp(-b(\Theta_{\min}-a))+1}}\right)\right)\right)dz}_{U_{14}} \right) \tag{58}$$

and $L_{34}(z) = \frac{2}{\sqrt{z}}e^{\frac{3\tilde{A}}{2}}[e^{-\frac{\tilde{A}}{2}}\sqrt{\frac{D_{min}^2 z}{\tilde{C}}}\mathrm{Ei}(\ln(\frac{D_{min}^2 z}{\tilde{C}}) - \tilde{A}) - \mathrm{Ei}(\frac{-3}{2}(\tilde{A} - \ln(\frac{D_{min}^2 z}{\tilde{C}})))]$.

APPENDIX I
PROOF OF REMARK 5

When $\tilde{C} \gg 1$, i.e., $P/\sigma^2 \gg 1$, similar with before, by using $\mathrm{erf}(x) \to 1$ when $x \to \infty$ and $\mathrm{erfc}(x) = 1 - \mathrm{erf}(x)$, one can get $\bar{\eta}_{LB}^{3D} \to R_s$, which completes the proof.

REFERENCES

[1] Y. Zeng, R. Zhang, and T. J. Lim, "Wireless communications with unmanned aerial vehicles: Opportunities and challenges," *IEEE Commun. Mag.*, vol. 54, no. 5, pp. 36–42, May 2016.

[2] Y. Ji, Z. Yang, H. Shen, W. Xu, K. Wang, and X. Dong, "Multicell edge coverage enhancement using mobile UAV-relay," *IEEE Internet Things J.*, vol. 7, no. 8, pp. 7482–7494, Aug. 2020.

[3] Y. Zeng, R. Zhang, and T. J. Lim, "Throughput maximization for UAV-enabled mobile relaying systems," *IEEE Trans. Commun.*, vol. 64, no. 12, pp. 4983–4996, Dec. 2016.

[4] Y. Zeng and R. Zhang, "Energy-efficient UAV communication with trajectory optimization," *IEEE Trans. Wireless Commun.*, vol. 16, no. 6, pp. 3747–3760, Jun. 2017.

[5] Q. Wu, Y. Zeng, and R. Zhang, "Joint trajectory and communication design for multi-UAV enabled wireless networks," *IEEE Trans. Wireless Commun.*, vol. 17, no. 3, pp. 2109–2121, Mar. 2018.

[6] A. Al-Hourani, S. Kandeepan, and S. Lardner, "Optimal LAP altitude for maximum coverage," *IEEE Wireless Commun. Lett.*, vol. 3, no. 6, pp. 569–572, Dec. 2014.

[7] M. Mozaffari, W. Saad, M. Bennis, and M. Debbah, "Efficient deployment of multiple unmanned aerial vehicles for optimal wireless coverage," *IEEE Commun. Lett.*, vol. 20, no. 8, pp. 1647–1650, Aug. 2016.

[8] M. Alzenad, A. El-Keyi, F. Lagum, and H. Yanikomeroglu, "3-D placement of an unmanned aerial vehicle base station (UAV-BS) for energy-efficient maximal coverage," *IEEE Wireless Commun. Lett.*, vol. 6, no. 4, pp. 434–437, Aug. 2017.

[9] Y. Zhou *et al.*, "Secure communications for UAV-enabled mobile edge computing systems," *IEEE Trans. Commun.*, vol. 68, no. 1, pp. 376–388, Jan. 2020.

[10] Y. Wang, Z.-Y. Ru, K. Wang, and P.-Q. Huang, "Joint deployment and task scheduling optimization for large-scale mobile users in multi-UAV-enabled mobile edge computing," *IEEE Trans. Cybern.*, vol. 50, no. 9, pp. 3984–3997, Sep. 2020

[11] C. She, C. Yang, and T. Q. S. Quek, "Cross-layer optimization for ultra-reliable and low-latency radio access networks," *IEEE Trans. Wireless Commun.*, vol. 17, no. 1, pp. 127–141, Jan. 2018.

[12] C. She, C. Liu, T. Q. S. Quek, C. Yang, and Y. Li, "Ultra-reliable and low-latency communications in unmanned aerial vehicle communication systems," *IEEE Trans. Commun.*, vol. 67, no. 5, pp. 3768–3781, May 2019.

[13] C. Pan, H. Ren, Y. Deng, M. Elkashlan, and A. Nallanathan, "Joint blocklength and location optimization for URLLC-enabled UAV relay systems," *IEEE Commun. Lett.*, vol. 23, no. 3, pp. 498–501, Mar. 2019.

[14] H. Ren, C. Pan, K. Wang, W. Xu, M. Elkashlan, and A. Nallanathan, "Joint transmit power and placement optimization for URLLC-enabled UAV relay systems," *IEEE Trans. Veh. Technol.*, vol. 69, no. 7, pp. 8003–8007, Jul. 2020.

[15] Y. Polyanskiy, H. V. Poor, and S. Verdu, "Channel coding rate in the finite blocklength regime," *IEEE Trans. Inf. Theory*, vol. 56, no. 5, pp. 2307–2359, May 2010.

[16] J. Ye, C. Zhang, H. Lei, G. Pan, and Z. Ding, "Secure UAV-to-UAV systems with spatially random UAVs," *IEEE Wireless Commun. Lett.*, vol. 8, no. 2, pp. 564–567, Apr. 2019.

[17] H. Ren, C. Pan, K. Wang, Y. Deng, M. Elkashlan, and A. Nallanathan, "Achievable data rate for URLLC-enabled UAV systems with 3-D channel model," *IEEE Wireless Commun. Lett.*, vol. 8, no. 6, pp. 1587–1590, Dec. 2019.

[18] A. A. Khuwaja, Y. Chen, N. Zhao, M.-S. Alouini, and P. Dobbins, "A survey of channel modeling for UAV communications," *IEEE Commun. Surveys Tuts.*, vol. 20, no. 4, pp. 2804–2821, 4th Quart., 2018.

[19] C. E. Shannon, "A mathematical theory of communication," *Bell Syst. Tech. J.*, vol. 27, no. 3, pp. 379–423, Jul./Oct. 1948.

[20] G. Durisi, T. Koch, and P. Popovski, "Toward massive, ultrareliable, and low-latency wireless communication with short packets," *Proc. IEEE*, vol. 104, no. 9, pp. 1711–1726, Sep. 2016.

[21] M. Abramowitz and I. A. Stegun, *Handbook of Mathematical Functions: With Formulas, Graphs, and Mathematical Tables* (National Bureau of Standards Applied Mathematics Series 55), 9th ed. Washington, DC, USA: U.S. Department of Commerce, 1972. [Online]. Available: http://people.math.sfu.ca/~cbm/aands/abramowitz_and_stegun.pdf

[22] Wolfram Research, Inc. *Complementary Error Function*. Accessed: Aug. 1, 2019. [Online]. Available: http://functions.wolfram.com/GammaBetaErf/Erfc/21/01/02/04/01/

[23] Wolfram Research. *Mathematica, Version 11.0*. Accessed: Aug. 1, 2019. [Online]. Available: https://www.wolfram.com/mathematica

[24] R. I. Bor-Yaliniz, A. El-Keyi, and H. Yanikomeroglu, "Efficient 3-D placement of an aerial base station in next generation cellular networks," in *Proc. IEEE Int. Conf. Commun. (ICC)*, May 2016, pp. 1–5.

[25] S. Boyd and L. Vandenberghe, *Convex Optimization*. Cambridge, U.K.: Cambridge Univ. Press, 2004.

[26] A. G. Glen, L. M. Leemis, and J. H. Drew, "Computing the distribution of the product of two continuous random variables," *Comput. Statist. Data Anal.*, vol. 44, no. 3, pp. 451–464, Jan. 2004.

[27] Wolfram Research, Inc. *Exponential Function*. Accessed: Aug. 1, 2019. [Online]. Available: http://functions.wolfram.com/ElementaryFunctions/Exp/21/01/02/02/02/.

[28] Wolfram Research, Inc. *Expintegralei Function*. Accessed: Aug. 1, 2019. [Online]. Available: http://functions.wolfram.com/GammaBetaErf/ExpIntegralEi/21/01/

Kezhi Wang (Senior Member, IEEE) received the B.E. and M.E. degrees from the School of Automation, Chongqing University, China, in 2008 and 2011, respectively, and the Ph.D. degree in engineering from the University of Warwick, U.K., in 2015. He was a Senior Research Officer of the University of Essex, U.K., from 2015 to 2017. He is currently a Senior Lecturer with the Department of Computer and Information Sciences, Northumbria University, U.K. His research interests include mobile edge computing, intelligent reflection surface (IRS), and machine learning.

Cunhua Pan (Member, IEEE) received the B.S. and Ph.D. degrees from the School of Information Science and Engineering, Southeast University, Nanjing, China, in 2010 and 2015, respectively. From 2015 to 2016, he was a Research Associate with the University of Kent, U.K.

He held a post-doctoral position with the Queen Mary University of London, U.K., from 2016 and 2019, where he is currently a Lecturer. His research interests mainly include intelligent reflection surface (IRS), machine learning, UAV, Internet of Things, and mobile edge computing. He serves as a TPC member for numerous conferences, such as ICC and GLOBECOM, and the Student Travel Grant Chair for ICC 2019. He also serves as an Editor for IEEE WIRELESS COMMUNICATION LETTERS, IEEE COMMUNICATION LETTERS, and IEEE ACCESS.

Hong Ren received the B.S. degree in electrical engineering from Southwest Jiaotong University, Chengdu, China, in 2011, and the M.S. and Ph.D. degrees in electrical engineering from Southeast University, Nanjing, China, in 2014 and 2018, respectively. From October 2016 to January 2018, she was a visiting student with the School of Electronics and Computer Science, University of Southampton, U.K. She is currently a Post-Doctoral Scholar with the School of Electronic Engineering and Computer Science, Queen Mary University of London, U.K. Her research interests lie in the areas of communication and signal processing, including cooperative transmission, Internet of Things, as well as ultra-reliability and low latency communications.

Wei Xu (Senior Member, IEEE) received the B.Sc. degree in electrical engineering and the M.S. and Ph.D. degrees in communication and information engineering from Southeast University, Nanjing, China in 2003, 2006, and 2009, respectively. From 2009 to 2010, he was a Post-Doctoral Research Fellow with the Department of Electrical and Computer Engineering, University of Victoria, Canada. He is currently a Professor at the National Mobile Communications Research Laboratory, Southeast University. He is also an Adjunct Professor of the University of Victoria, Canada, and a Distinguished Visiting Fellow of the Royal Academy of Engineering, U.K. He has coauthored over 100 refereed journal papers in addition to 36 domestic patents and four US patents granted. His research interests include cooperative communications, information theory, signal processing, and machine learning for wireless communications. He received the Best Paper Awards from IEEE MAPE 2013, IEEE/CIC ICCC 2014, IEEE Globecom 2014, IEEE ICUWB 2016, WCSP 2017, and ISWCS 2018. He was a co-recipient of the First Prize of the Science and Technology Award in Jiangsu Province, China, in 2014. He received the Youth Science and Technology Award of the China Institute of Communications in 2018. He was an Editor of IEEE COMMUNICATIONS LETTERS from 2012 to 2017. He is currently an Editor of IEEE TRANSACTIONS ON COMMUNICATIONS and IEEE ACCESS.

Lei Zhang (Senior Member, IEEE) is currently a Senior Lecturer with the University of Glasgow, U.K. He has 19 patents granted/filed in more than 30 countries/regions. He has published two books and over 100 peer-reviewed papers. His research interests include wireless communication systems and networks, blockchain technology, as well as data privacy and security. He received the IEEE ComSoc TAOS Best Paper Award 2019. He is a Technical Committee Chair of the 5th International Conference on UK-China Emerging Technologies (UCET) 2020. He is an Associate Editor of IEEE INTERNET OF THINGS (IoT) Journal, IEEE WIRELESS COMMUNICATIONS LETTERS, and *Digital Communications and Networks*.

Arumugam Nallanathan (Fellow, IEEE) was with the Department of Informatics, King's College London, from December 2007 to August 2017, where he was a Professor of Wireless Communications from April 2013 to August 2017 and has been a Visiting Professor since September 2017. He was an Assistant Professor with the Department of Electrical and Computer Engineering, National University of Singapore, from August 2000 to December 2007. He is currently a Professor of Wireless Communications and the Head of the Communication Systems Research (CSR) Group, School of Electronic Engineering and Computer Science, Queen Mary University of London, since September 2017. He has published nearly 500 technical papers in scientific journals and international conferences. He has been selected as a Web of Science Highly Cited Researcher in 2016. His research interests include Artificial Intelligence for Wireless Systems, Beyond 5G Wireless Networks, Internet of Things (IoT), and Molecular Communications.

Dr. Nallanathan is a co-recipient of the Best Paper Awards presented at the IEEE International Conference on Communications 2016 (ICC'2016), IEEE Global Communications Conference 2017 (GLOBECOM'2017), and IEEE Vehicular Technology Conference 2018 (VTC'2018). He has served as the Chair for the Signal Processing and Communication Electronics Technical Committee of IEEE Communications Society and Technical Program Chair and a member of Technical Program Committees in numerous IEEE conferences. He received the IEEE Communications Society SPCE Outstanding Service Award 2012 and IEEE Communications Society RCC Outstanding Service Award 2014. He is an Editor of IEEE TRANSACTIONS ON COMMUNICATIONS. He was an Editor of IEEE TRANSACTIONS ON WIRELESS COMMUNICATIONS (2006–2011), IEEE TRANSACTIONS ON VEHICULAR TECHNOLOGY (2006–2017), IEEE WIRELESS COMMUNICATIONS LETTERS, and IEEE SIGNAL PROCESSING LETTERS. He is an IEEE Distinguished Lecturer.